Technol. Biotechnol. **1992**, *53* (3), 237-242.
Komasawa, I.; Otake, T.; Higaki, Y. Equilibrium Studies of the Extraction of Divalent Metals from Nitrate Media with Di(2-ethylhexyl)phosphoric Acid. *J. Inorg. Nucl. Chem.* **1981**, *43* (12), 3351-3356.
Li, Y. G.; Lu, J. F.; Li, Z. C.; Bao, T. Z.; Li, J. D.; Teng, T. Determination of Thermodynamic Equilibrium Constants and Activity Coefficients for Metal Solvent Extraction Systems. In *Separation Processes in Hydrometallurgy*; Davies, G. A.; Ed.; Ellis Horwood: West Sussex, U.K., 1987; Part 2, Chapter 24.
Morel, F. M. M. *Principles of Aquatic Chemistry*; Wiley-Interscience: New York, 1983; pp 242-249.
Peppard, D. F.; Ferraeo, J. R.; Mason, G. W. Hydrogen Bonding in Organophosphoric Acids. *J. Inorg. Nucl. Chem.* **1958**, *7*, 231-244.
Pitzer, K. S.; Mayorga, G. Thermodynamics of Electrolytes. II. Activity and Osmotic Coefficients for Strong Electrolytes with One or Both Ions Univalent. *J. Phys. Chem.* **1973**, *77*, 2300-2308.
Pitzer, K. S.; Kim, J. J. Thermodynamics of Electrolytes. IV. Activity and Osmotic Coefficients for Mixed Electrolytes. *J. Am. Chem. Soc.* **1974**, *96*, 5701-5707.
Pitzer, K. S.; Mayorga, G. Thermodynamics of Electrolytes. III. Activity and Osmotic Coefficients for 2-2 Electrolytes. *J. Solution Chem.* **1974**, *3*, 539-546.
Pitzer, K. S.; Roy, R. N.; Silvester, L. F. Thermodynamics of Electrolytes. 7. Sulfuric Acid. *J. Am. Chem. Soc.* **1977**, *99*, 4930-4936.
Sato, T.; Nakamura, T. The Stability Constants of the Aqueous Chloro-Complexes of Divalent Zinc, Cadmium and Mercury Determined by Solvent Extraction with Tri-*n*-octylphosphine Oxide. *Hydrometallurgy* **1980**, *6*, 3-12.
Tanaka, M. Modelling of Solvent Extraction Equilibria of Cu(II) from Nitric and Hydrochloric Acid Solutions with β-Hydroxyoxime. *Hydrometallurgy* **1990**, *24*, 317-331.
Whewell, R. J.; Hughes, M. A. The Modelling of Equilibrium Data for the Liquid-Liquid Extraction of Metals. III. An Improved Chemical Model for the Copper/LIX64N System. *Hydrometallurgy* **1979**, *4*, 109-124.

Received for review March 16, 1992
Accepted July 6, 1992

Thermal Conductivities of Molten Alkali Metal Halides

Makoto Harada, Akihisa Shioi,* Tsunetoshi Miura, and Shinsuke Okumi
Research Section of Nuclear Chemical Engineering, Institute of Atomic Energy, Kyoto University, Uji, Kyoto 611, Japan

Thermal conductivities of molten alkali metal halides were measured by two kinds of laser flash methods for three-layered systems (metal disk/sample liquid/metal disk). One is to measure the temperature response at the front surface of the upper metal disk below which sample liquid layer was located, and the other is to measure the temperature response at the rear surface of the lower metal disk above which the sample liquid and the upper metal disk layers are present. The effect of radiation on the temperature response was explicitly taken into account. The thermal conductivities obtained by the two methods agreed with each other within the experimental precision, and the reproducibility of the data was within 10%. The thermal conductivities of molten alkali metal halides showed a weak negative temperature dependence. The corresponding-states correlation for the thermal conductivity was also presented using the data reported in the present work.

1. Introduction

Molten alkali metal halides are typical uni-univalent ionic liquids. Their equilibrium properties are expressed using the pair potential comprised of the electrostatic and the core repulsive interactions. Then, the corresponding-states correlations for the equilibrium properties are given by a function of two state variables, the reduced temperature and the reduced density (Reiss et al., 1961; Harada et al., 1983). The corresponding-states correlations for transport properties have been studied by several investigators (White and Davis, 1967; Young and O'Connell, 1971). Tada et al. (1988) reported the corresponding-states correlations for the transport properties by taking into account the mass difference between the cation and the anion, and showed that the electric conductivities and the viscosities of alkali metal halides are successfully correlated by their theory. The validity of the corresponding-states correlation is unknown for the thermal conductivity, because the thermal conductivities of molten alkali metal halides reported by several researchers strongly disagree with each other.

The accurate measurement of the thermal conductivity is quite difficult for molten alkali metal halides due to their high melting points, large electric conductivity, and rather strong chemical activity. Radiative and convective heat transport play a significant role at high temperature. The high electric conductivity makes the application of Joule heating as the heat source difficult. The strong chemical activity restricts the materials used for a sample liquid container. The thermal conductivities reported for molten potassium chloride (McDonald and Davis, 1971; Fedorov and Machuev, 1970; Polyakov and Gildebrandt, 1974; Bystrai et al., 1974; Nagasaka and Nagashima, 1988) are widely scattering within several hundred percent.

Harada and co-workers (Harada et al., 1985; Tada et al., 1978, 1981) developed the laser flash method (LF) to measure the thermal conductivities of liquids and extended it to the measurement under the condition of elevated temperature. They used the two-layer system composed of a metal disk and a sample liquid layer. The laser beam was impulsively flashed on the metal disk, and the thermal conductivity was obtained from the temperature response at the front surface of the metal disk. We call this method LF-I. Lee and Taylor (1978) applied the laser flash method to the measurement for liquids. They used a three-layer system, i.e., metal disk/sample liquid/metal disk. The thermal conductivity was obtained from the temperature response at the rear metal disk. This method (abbreviated as LF-II) is essentially the same as that proposed by Parker et al. (1961). These two methods (LF-I and LF-II) are suited for the measurement of the thermal conductivities of molten alkali metal halides, because no special liquid container and no Joule heating are needed. It is important to elucidate how radiation affects the measurement when applying these methods to the measurement for high-temperature liquids.

In this work, we applied the two kinds of LF (LF-I and LF-II) to measuring the thermal conductivities of some molten alkali metal halides, i.e., NaCl, NaBr, NaI, KCl, KBr, KI, RbCl, RbBr, and RbI. The effect of the radiation

0888-5885/92/2631-2400$03.00/0

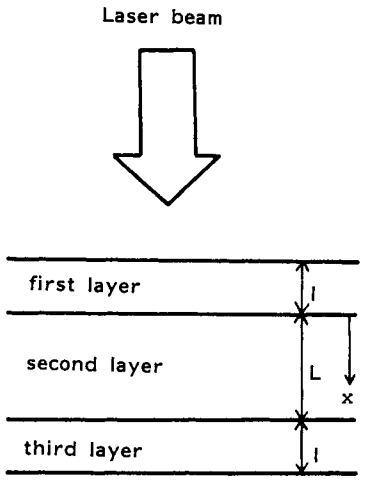

Figure 1. Schematic diagram of geometry.

on the heat transport was taken into account in both methods. The corresponding-states correlation for the thermal conductivity was obtained using the data presented in this work.

2. Principles of Measurement

Consider the three-layer system shown in Figure 1. The laser beam is impulsively flashed onto the front surface of the first layer made of a thin metal disk. The heat accumulated in the first layer discharges to the second layer (sample liquid) and then to the third layer. In the LF-I case, the second layer is designed so that the heat penetration length is less than the thickness of the second layer; i.e., the third layer acts as a sample holder. In LF-II, the third layer is a thin metal disk which is made of the same materials and has the same geometry as the first layer.

We postulate as follows: (1) The heat flow in question is one dimensional. (2) The temperature in the metal disks is uniform because their thermal conductivity is very high compared with the sample liquid and their thicknesses, l, is so small. (3) The sample liquid is optically very thin. (4) The temperature rise after flashing the laser beam is so small that the physical properties of the materials are invariant regardless of the temperature change. (5) The heat flux from the metal disk to the atmosphere is proportional to the temperature rise of the metal disk. (6) The radiation heat flux from the first to the third layer is proportional to the temperature difference between the two layers. This radiation flux is proportional to $(T + T_1)^4 - (T + T_3)^4$, where T_i and T, respectively, are the temperature rise of the ith layer and the temperature before flashing the laser pulse. When T_1 and $T_3 \ll T$, the heat flux is proportional to $(T_1 - T_3)$ as an approximation. Then, postulation 6 is justifiable.

2.1. LF-I Case. This method is essentially the same as that reported by Tada et al. (1978). However, the heat discharge process from the metal disk to the atmosphere by radiation, which is not considered in the previous work, becomes important in the present case. Considering the semi-infinite second layer, the equations governing the heat transport and the corresponding initial and boundary conditions are described:

$$d_1C_{P1}l\ \mathrm{d}T_1/\mathrm{d}t = \lambda_2(\partial T_2/\partial x)_{x=0} - RT_1 \tag{1}$$

$$d_2C_{P2}\ \partial T_2/\partial t = \lambda_2\ \partial^2T_2/\partial x^2 \tag{2}$$

initial conditions

$$T_1 = T^* \quad \text{and} \quad T_2 = 0 \quad \text{at} \quad t = 0 \tag{3}$$

boundary conditions

$$T_2 = T_1 \quad \text{at} \quad x = 0 \tag{4}$$

$$T_2 = 0 \quad \text{at} \quad x = \infty \tag{5}$$

Here, t is time; x is the distance measured from the rear surface of the first layer. T_i is the temperature rise in the ith layer due to flashing the laser pulse. d_i, C_{Pi}, and λ_i are the density, the specific heat, and the thermal conductivity of the ith layer, respectively. R is the parameter concerning the heat discharge processes from the first layer to the atmosphere. The R value is proportional to the third power of the temperature in the first layer before flashing a laser pulse, when the radiation dominates R.

From the governing equations, the Laplace transform of T_1, $\tilde{T}_1$, is derived as

$$s\tilde{T}_1 - T^* + H\tilde{T}_1 + h\,s^{1/2}\tilde{T}_1 = 0 \tag{6}$$

where

$$H = R/(d_1C_{P1}l), \quad h = \beta_2\,D_2^{1/2},$$
$$\beta_2 = d_2C_{P2}/(d_1C_{P1}l), \quad D_2 = \lambda_2/(d_2C_{P2})$$

s is the argument of the Laplace transform. The inverse transform of each term of eq 6 yields

$$\mathrm{d}T_1/\mathrm{d}t + HT_1 + h(\mathrm{d}/\mathrm{d}t)\int_0^t T_1(\tau)\{\pi(t-\tau)\}^{-1/2}\,\mathrm{d}\tau = 0 \tag{7}$$

Integration of eq 7 reduces to

$$Y(t) = hX(t) + H \tag{8}$$

Here

$$Y(t) = \{1 - T_1(t)/T^*\}/\int_0^t \{T_1(\tau)/T^*\}\,\mathrm{d}\tau \tag{9}$$

and

$$X(t) = \frac{2\{t/\pi\}^{1/2}\int_0^1 T_1(t(1-u^2))/T^*\,\mathrm{d}u}{\int_0^t \{T_1(\tau)/T^*\}\,\mathrm{d}\tau} \tag{10}$$

$X(t)$ and $Y(t)$ are obtained from the temperature response $T_1(t)/T^*$. The thermal diffusivity of a sample liquid D_2 is determined from the slope h of the straight line of $Y(t)$ against $X(t)$.

2.2. LF-II Case. The equations governing the heat transport and the corresponding initial and boundary conditions are expressed by

$$d_1C_{P1}l\ \mathrm{d}T_1/\mathrm{d}t = \lambda_2(\partial T_2/\partial x)_{x=0} - RT_1 - R'(T_1 - T_3) \tag{11}$$

$$d_2C_{P2}\ \partial T_2/\partial t = \lambda_2\ \partial^2T_2/\partial x^2 \tag{12}$$

$$d_1C_{P1}l\ \mathrm{d}T_3/\mathrm{d}t = -\lambda_2(\partial T_2/\partial x)_{x=L} - RT_3 + R'(T_1 - T_3) \tag{13}$$

initial conditions

$$T_1 = T^*, \quad T_2 = T_3 = 0 \quad \text{at} \quad t = 0 \tag{14}$$

boundary conditions

$$T_2 = T_1 \quad \text{at} \quad x = 0 \tag{15}$$

$$T_2 = T_3 \quad \text{at} \quad x = L \tag{16}$$

Here R' is the parameter concerned with the radiation from the first to the third layer and L is the thickness of the

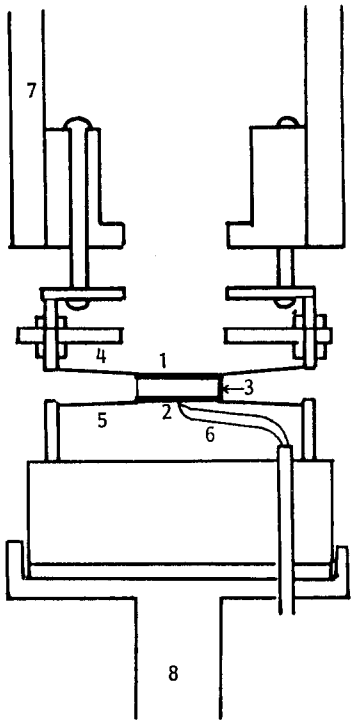

Figure 2. Detailed description of measuring device for LF-II: 1, platinum disk (upper); 2, platinum disk (lower); 3, quartz chips; 4 and 5, platinum wire; 6, Pt–Pt/13% Rh thermocouple; 7, upper rod; 8, support rod.

second layer. The other notations are the same as those for LF-I.

The Laplace transform of $T_3(t)$, $\bar{T}_3$, is expressed by

$$\bar{T}_3/T^* = [2\beta_2(D_2s)^{1/2} + H'\{\exp(L(s/D_2)^{1/2}) - \exp(-L(s/D_2)^{1/2})\}]/[\exp(L(s/D_2)^{1/2})\{s + H + H' + \beta_2(D_2s)^{1/2} - H'\exp(-L(s/D_2)^{1/2})\}^2 - \exp(-L(s/D_2)^{1/2})\{s + H + H' - \beta_2(D_2s)^{1/2} - H'\exp(L(s/D_2)^{1/2})\}^2] \quad (17)$$

This equation is approximated in the short term, $L(s/D_2)^{1/2} \gg 1$:

$$Z = \exp(-L(s/D_2)^{1/2}) \quad (18)$$

Here, Z is defined by

$$Z \equiv [(\bar{T}_3/T^*)(s + H + \beta_2(D_2s)^{1/2}) \times (s + H + 2H' + \beta_2(D_2s)^{1/2}) - H']/(2\beta_2(D_2s)^{1/2}) \quad (18')$$

Here, $H' = R'/(d_1C_{P1}l)$ and the other notations are the same as those for LF-I. The temperature response in the long term, $L(s/D_2)^{1/2} \ll 1$, is given by

$$T_3(t) = \{T^*d_1C_{P1}l/(2d_1C_{P1}l + d_2C_{P2}L)\} \times \exp[-Ht/\{1 + (d_2C_{P2}L)/(2d_1C_{P1}l)\}] \quad (19)$$

We obtain T^* and H values from the long-term response of $T_3(t)$. The thermal diffusivities of the sample liquid D_2 and H' values are determined from the short-term response of $T_3(t)$ with the help of the corresponding T^* and H values.

3. Experimental Section

3.1. Apparatus. 3.1.1. LF-I Method. The experimental setup and the essential part of the measuring device for LF-I are essentially the same as those in a previous work (Tada et al., 1981). In the present case, the sample was fed in the sample holder as the powder. Then, the sample powder was carefully dried at the temperature that was lower by 50 °C than the melting point. After the sample powder was melted and was attained to a requisite temperature, the measurement was carried out.

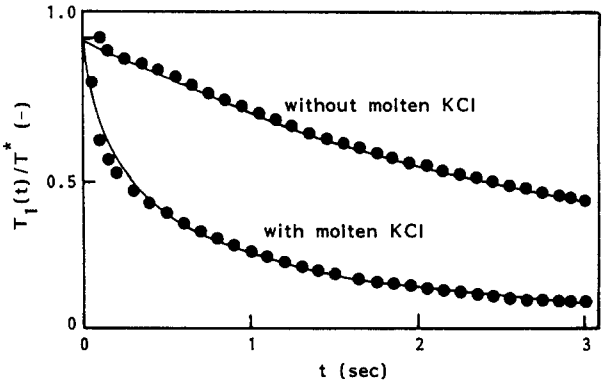

Figure 3. Examples of temperature responses with and without molten KCl. The temperature before laser flash is 1098.6 K. Laser intensities in the two cases are equal to each other. The solid curves are calculated from eq 20 (without molten KCl) and from the inverse Laplace transform of eq 6 (with molten KCl).

A ruby laser with a maximum energy of 6 J per pulse was used. The pulse duration was less than 0.5 ms and was neglected for evaluating the thermal conductivity. The beam diameter was 10 mm, and the ruby rod was cooled by water. The intensity of the laser beam was measured by the detector with the aid of a semitransparent mirror. The X and Y values were calculated by an on-line personal computer.

3.1.2. LF-II Method. The experimental apparatus and the layout for LF-II were almost the same as in the LF-I case. The measuring device, which was somewhat different from that for the LF-I case, is shown in Figure 2. The two metal disks 1 and 2 made of platinum were 8 mm in diameter and 0.2 mm in thickness. The upper metal disk was fixed to the upper rod 7 with three platinum wires 4 (0.2-mm diameter), and the lower metal disk was supported to the rod 8 with three platinum wires (0.2-mm diameter) 5. The wires were spot-welded on the peripheries of the metal disks. The distance between two metal disks was controlled by inserting three quartz chips (~0.5-mm height) 3 between them. The sample liquid was sandwiched between two metal disks. The laser beam was impulsively flashed onto the front surface of the upper disk 1. The Pt–Pt/13% Rh thermocouple 6 was spot-welded on the rear surface of the lower disk 2 to measure the temperature response.

A requisite amount of the sample powder on the lower metal disk was dried in the same way as in the LF-I case and then melted. The liquid level was confirmed to agree with the level of the top of the quartz chips when the sample powder melted. After the temperature of the sample was attained to a requisite value, the lower disk was raised until the top of the quartz chips just touched the rear surface of the upper disk.

The maximum temperature rise, i.e., T^* value, was set within 5 K in both methods so that postulations 4, 5, and 6 were satisfied. The platinum metal disks used in the present work were thin enough for the metal disks to be regarded as heat capacitors of uniform temperatures.

3.2. Materials. The alkali metal halides and sodium nitrates employed in this work were of reagent grade (purity over 99.5%). The platinum plate was supplied from Nilaco Corporation (purity over 99.98%).

4. Results

4.1. Temperature Response in LF-I Method. The thermal conductivities of alkali metal nitrates measured

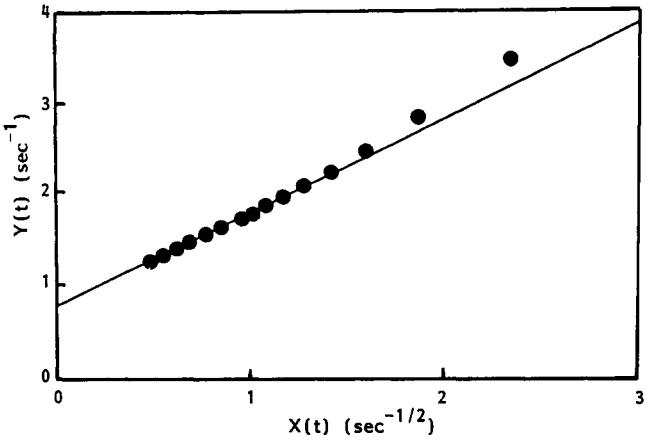

Figure 4. Plots of $Y(t)$ against $X(t)$ for the response for KCl shown in Figure 3.

by the LF-I method have been reported elsewhere (Tada et al., 1981), and we present here a typical example of the temperature response measured for KCl.

Figure 3 shows the temperature responses of $T_1(t)$ in the cases with and without molten KCl. These responses were measured at the same temperature and at the same laser intensity. The temperature responses in Figure 3 are normalized with T^*, which is determined from the temperature response of the metal disk without sample liquid:

$$T_1(t)/T^* = \exp(-Ht) \tag{20}$$

The solid curve in Figure 3, which is calculated from eq 20, explains well the response without KCl. Thus, postulation 5 is satisfied in our experiments, and we can obtain the T^* value from the data in the liquid-free case with the help of eq 20. The relationship between $X(t)$ and $Y(t)$ for the experimental result for KCl is plotted in Figure 4. A linear relationship is established between $X(t)$ and $Y(t)$, indicating that the experiment satisfied the conditions of eq 8. The weak deviation of the data from the straight line in the large $X(t)$ region, i.e., in the short-term region, is probably attributed to the nonuniform temperature rise in the radial direction of the metal disk, which is caused by the intensity distribution in the cross section of the laser beam. Nevertheless, this unwelcome phenomenon is not crucial because the large thermal diffusivity of the metal disk rapidly eliminates the nonuniform temperature distribution. The solid curve for the KCl case in Figure 3 is calculated from the inverse Laplace transform of eq 6 (Harada et al., 1985) with the h and H values obtained from Figure 4. The small disagreement caused by the nonuniform temperature rise is observed in the extremely short term region, but the calculated curve fits well the observed data except for this region, showing the validity of postulation 1.

4.2. Temperature Responses in LF-II Method. The thermal conductivities of molten alkali metal nitrates have been extensively measured by several investigators, and we first checked the validity of the LF-II method using sodium nitrate. An example of the response of $T_3(t)$ for molten sodium nitrate is shown in Figure 5a. As shown in Figure 5b, a linear relationship between ln $[T_3(t)]$ and t is obtained for the long-term response, indicating the validity of eq 19. The H and T^* values are evaluated from the slope of this straight line in Figure 5b and from its intercept at $t = 0$ with the help of the heat capacities $C_{P1}d_1$ and $C_{P2}d_2$. Here, $C_{P2}d_2$ is the average for the sample liquid and the quartz chips.

The thermal diffusivity was calculated as follows: (1) We assume D_2 and H' values, and calculate ln Z with the

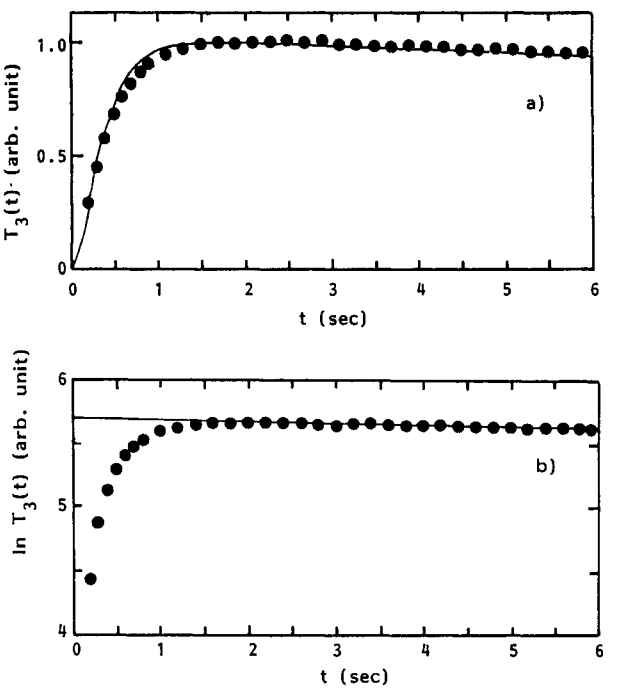

Figure 5. Example of $T_3(t)$ for molten $NaNO_3$ at 688.2 K. (a) $T_3(t)$ values are normalized by the maximum temperature. The solid curve is the numerical solution by the Cranck–Nicholson algorithm. (b) ln $T_3(t)$ against t.

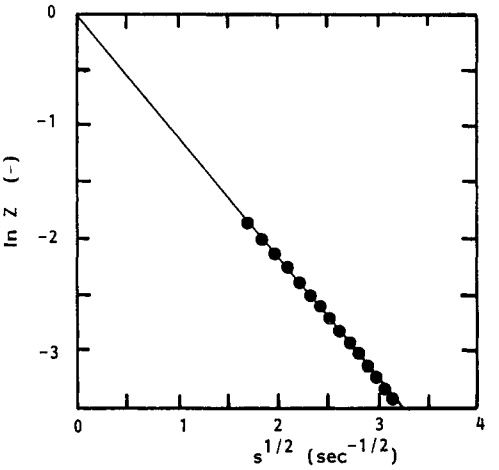

Figure 6. ln Z values against $s^{1/2}$ for the response in Figure 5.

help of the H and T^* values. (2) A renewed D_2 value is obtained from the slope of the line of ln Z against $s^{1/2}$, and then we calculate a renewed Z value using the renewed D_2 value. (3) The iteration procedure is repeated until the D_2 value converges. (4) Unless the line between ln Z and $s^{1/2}$ thus obtained passes through the origin (ln Z = $s^{1/2}$ = 0), a renewed H' value is postulated, and the converged D_2 value is newly obtained. (5) The above procedure, 1–4, is repeated until the line of ln Z against $s^{1/2}$ passes through the origin.

Figure 6 shows the final relationship between ln Z and $s^{1/2}$ for the result shown in Figure 5a. The short-term response (the data points from $t = 0$ to several hundred milliseconds) primarily affects the part of large s values. The linear relationship observed in Figure 6 indicates the validity of eq 18. The solid curve shown in Figure 5a is the numerical solution of eqs 11–16 with the H, T^*, D_2, and H' values obtained from the above procedures, using the Cranck–Nicholson algorithm. This curve fits well the observed data, but a small difference is observed in the

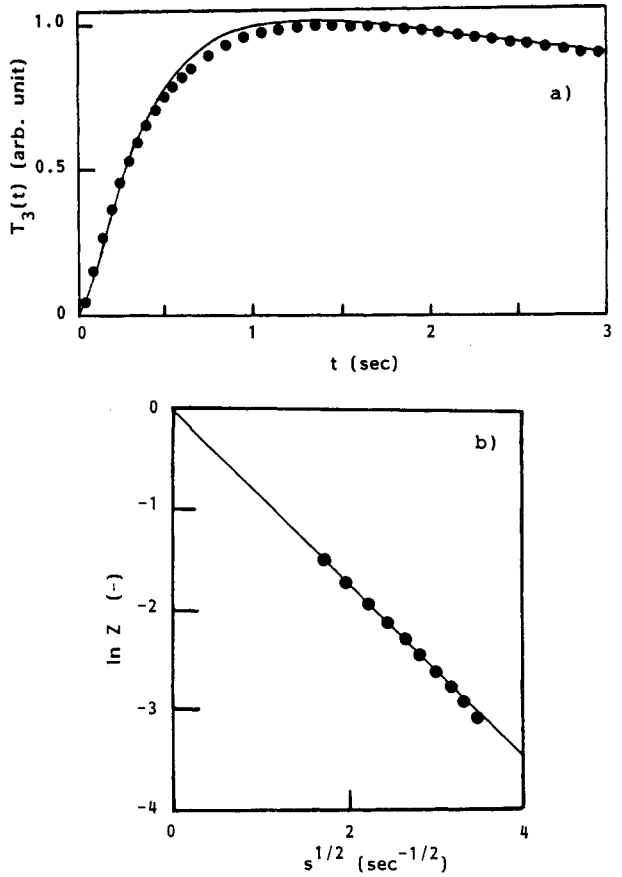

Figure 7. Example of the temperature response in LF-II for molten KCl. (a) $T_3(t)$ at 1099.2 K. $T_3(t)$ is normalized by the maximum temperature. The solid curve is the numerical solution by the Cranck–Nicholson algorithm. (b) Corresponding ln Z values against $s^{1/2}$.

middle part of the time scale. This difference is probably due to the temperature distribution toward the radial direction of the sample liquid, which is caused by the radiation from the periphery of the sample to the atmosphere. Since the temperature difference between the sample liquid and the atmosphere is small in the early stage of the temperature response, this phenomenon is not significant in the short-term response, which is essential for determining the thermal diffusivity. The good agreement between the calculated and the observed responses in the short time scale demonstrates that the measurement is carried out under the conditions of eqs 11–16 in this time scale. In long-term scale, the above radiation effect is also not so strong due to uniformity of the temperature.

The thermal conductivity of sodium nitrate obtained is 0.586 W/(m K). This value agrees with the data reported by White and Davis (1967) within the experimental error and is slightly higher than those of Kitade et al. (1989). Here, we used the published data for the density and the specific heat of molten $NaNO_3$ (Janz, 1967; Barin and Knacke, 1973) and for the density and the specific heat of platinum (Gray, 1972).

We also measured the thermal conductivity of water, which agreed with the recommended value (Makita, 1964) within 1.0%. The reproducibility of the thermal conductivities of water was very good even when we used the experimental conditions with different L values and different occupied area of the quartz chips. This shows that the heat flow through the quartz chips can be neglected, because the area occupied by the quartz chips was extremely small compared with the metal disk. Since the thermal diffusivities of water and molten salts are in the same order of magnitude, the heat flow through the quartz chips can be neglected for the measurement for molten salts.

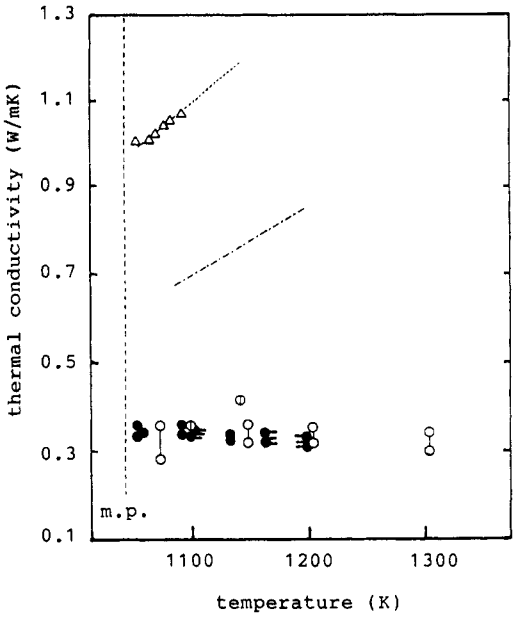

Figure 8. Thermal conductivity of molten KCl. ●, present work; ○, Nagasaka and Nagashima (1988); ⊙, McDonald and Davis (1971); △, Polyakov and Gildebrandt (1974); - - -, Bystrai et al. (1974); –·–, Fedorov and Machuev (1970). The dashed vertical line represents the melting point of KCl. Keys with – represent the values obtained by LF-I.

Figure 7 shows an example of the temperature response of $T_3(t)$ for molten KCl and the relationship between ln Z and $s^{1/2}$. The linear relationship is obtained in Figure 7b. The solid curve in Figure 7a is the numerical solution of eqs 11–16 using the Cranck–Nicholson algorithm. The agreement between the calculated and the observed data is good in the short term. However, a small difference between the calculated and the experimental values is observed in the middle time scale as in the case of molten $NaNO_3$. The difference in the case of molten KCl is a little larger than that in the case of molten $NaNO_3$, because of higher experimental temperatures for molten KCl.

4.3. Thermal Conductivities for Molten Alkali Metal Halides. The thermal conductivities of molten KCl obtained by LF-I and LF-II are presented in Figure 8 together with the published data. Here we used the published data of the density and the specific heat of molten KCl (Janz, 1967; Barin and Knacke, 1973). The agreement of the thermal conductivities by the two methods is satisfactory. The thermal conductivities obtained in the present work agree with the results obtained by the forced Rayleigh scattering method (Nagasaka and Nagashima, 1988) within the experimental error, and are a little smaller than the data reported by McDonald and Davis (1971). The thermal conductivities reported by Fedorov and Machuev (1970), Polyakov and Gildebrandt (1974), and Bystrai et al. (1974) are much larger than the present results.

The thermal conductivities of molten alkali metal halides obtained in the present work are shown in Figure 9. We used the densities and the specific heats of molten alkali metal halides reported in the same literature as that for molten KCl. Thermal conductivities for KCl, KBr, and RbCl obtained by the two methods agree well with each other within the experimental error. Thermal conductivities of molten alkali metal halides obtained by McDonald and Davis (1971) and Nakazawa et al. (1989,

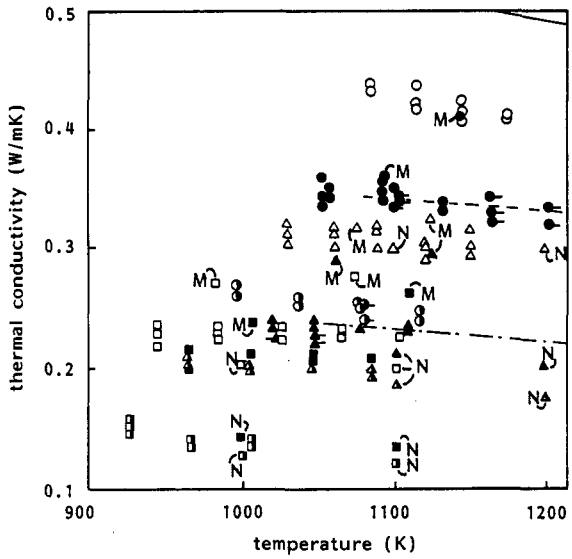

Figure 9. Comparison of the thermal conductivities of molten alkali halides obtained by the present work with the reported data. ○, NaCl; ●, KCl; ◑, RbCl; △, NaBr; ▲, KBr; ▲, RbBr; □, NaI; ■, KI; ◨, RbI. Keys with – represent the data obtained by LF-I. M and N represent the data reported by McDonald and Davis (1971) and Nakazawa et al. (1990), respectively. The various lines in this figure are the correlation reported by Nakazawa et al. (1989): —, NaCl; - - -, KCl; -·-, RbCl.

1990) are also shown in Figure 9. Thermal conductivities of molten alkali metal halides obtained in the present work show weak negative dependency on the temperature.

5. Corresponding-States Correlation

Following the Kubo formula (1957), the thermal conductivity of an isotropic liquid, λ, is expressed by the following equations

$$\lambda = (1/VkT^2)\int_0^\infty \langle \dot{A}(0)\,\dot{A}(t)\rangle\,dt \qquad (21)$$

and

$$A(t) = \sum_i r_{ix}\{\vec{P}_i^2/(2m_i) + \sum_{j>i}\phi_{ij}\}, \quad \dot{A}(t) = dA(t)/dt \qquad (22)$$

Here, V, k, and T are the volume of the system, the Boltzmann constant, and the temperature, respectively. $\vec{P}_i$ and m_i are the momentum r the mass of the ith ion. ϕ_{ij} is the pair potential between the ith and jth ions. r_{ix} is the x component of the position vector of the ith ion. ϕ_{ij} is expressed by

$$\phi_{ij}(r_{ij}) = \psi_{ij}\exp(-r_{ij}/\rho_{ij}) + Z_iZ_je^2\xi/r_{ij} \qquad (23a)$$

Here, the first term represents the core repulsive potentials, and the second term represents the Coulombic potentials. ψ_{ij}, ρ_{ij}, and ξ are the potential parameters. Z_i is the valence of the ith ion, and r_{ij} is the separation distance between the ith and jth ions. Since the pair potential for unlike ion pairs dominates the configuration of ions, the ψ_{ij} and ρ_{ij} values for unlike ion pairs are used even for the like ion pair. Thus, the pair potential is represented by

$$\phi_{ij}(r_{ij}) = \psi\exp(-r_{ij}/\rho) - e^2\xi/r_{ij} \qquad (23b)$$

where ψ and ρ are the values for unlike ion pairs given by Tosi and Fumi (1964).

The law of corresponding states is expressed for the thermal conductivity of uni-univalent ionic liquid (Tada et al., 1988):

$$\lambda^* = \lambda d^2/[k(\Lambda/m^*)^{1/2}] = \lambda_0^* + \sum_{n=1}^{\infty} S_{2n}\mu^{2n} \qquad (24)$$

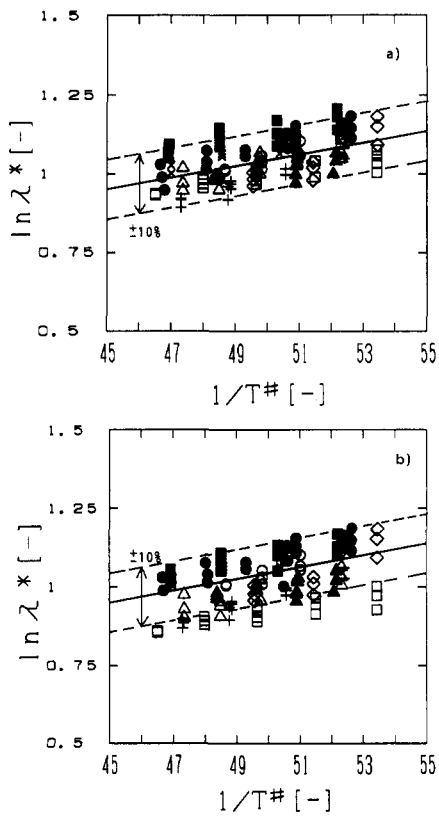

Figure 10. ln λ^* against $1/T^*$. ○, NaCl; ●, KCl; +, RbCl; △, NaBr; ▲, KBr; ×, RbBr; □, NaI; ■, KI; ◇, RbI. (a) $m^* = m_S$; (b) $m^* = m_R$. The solid line is calculated from eq 30.

Here, d is the characteristic separation distance between the anion and the cation, which is given by Harada et al. (1983):

$$d/\rho = \zeta\{0.4069 + 0.9075\ln(\psi/kT) + 6.042\times10^{-7}(\psi/kT)\} \qquad (25)$$

ζ is the parameter specific to salt species. Λ represents the core potential at $r = d$:

$$\Lambda = \psi\exp(-d/\rho) \qquad (26)$$

λ_0^* represents the reduced thermal conductivity for a hypothetical ionic liquid with a unique ionic mass m^*. The second term of the right-hand side of eq 24 is the perturbed term which arises from the mass difference μ between the anion and the cation.

The first choice for m^* and μ is based on the fact that the autocorrelation function in eq 21 is well expressed by the relative motion of the ion pairs in the short time scale:

$$m^* = m_R = 2m_Am_C/(m_A + m_C) \qquad (27a)$$

$$\mu = \mu_R = |m_A - m_C|/(m_A + m_C) \qquad (27b)$$

The second kind of m^*, m_S, is chosen so that the perturbed Hamiltonian of the system vanishes:

$$m^* = m_S = [2m_A^{1/2}m_C^{1/2}/(m_A^{1/2} + m_C^{1/2})]^2 \qquad (28a)$$

$$\mu = \mu_S = |m_A^{1/2} - m_C^{1/2}|/(m_A^{1/2} + m_C^{1/2}) \qquad (28b)$$

Figure 10a and Figure 10b show the corresponding-states correlations for the thermal conductivities of molten alkali metal halides using $m^* = m_S$ and $m^* = m_R$, respectively. The reduced temperature T^* is defined by

$$T^* = kTd/(e^2\xi) \qquad (29)$$

All the data used are obtained in the present work. The

parameters ψ, ρ, ξ, and ζ are shown elsewhere (Tada et al., 1988). The perturbed term of eq 24 plays a minor role in the correlation. The correlation with the help of m_S is a little better than that with m_R by referring to the thermal conductivities of NaI, in which the ionic mass difference is the largest. This has been observed for the electric conductivities and for the viscosities of molten alkali metal halides (Tada et al., 1988).

The reduced thermal conductivities of molten alkali metal halides are expressed by eq 30 within ±10%.

$$\lambda^* = \lambda d^2/[k(\Lambda/m_S)^{1/2}] = 1.122 \exp(0.01857/T^*) \quad (30)$$

The thermal conductivities of molten alkali metal halides decrease as the temperature increases.

6. Conclusions

Thermal conductivities of molten alkali metal halides were measured by two kinds of laser flash methods which explicitly take into account the effects of the radiation on heat transport. The agreement of the values obtained by the two methods is satisfactory. The reproducibility of the data was within 10%. The thermal conductivities obtained in the present work have negative temperature dependencies irrespective of the species. Corresponding-states correlation was presented. The change in the reduced thermal conductivity caused by the mass difference between anion and cation is negligibly small. The reduced thermal conductivities of molten alkali metal halides can be correlated using the interionic potential parameters which have been determined so that the equilibrium properties are well reproduced.

Acknowledgment

We thank Dr. M. Kinoshita (Associate Professor of Kyoto University) for his useful suggestions for obtaining the numerical solutions of eqs 11–16. The numerical calculations were carried out at the Data Processing Center, Kyoto University. We also thank Mr. M. Shibano for his assistance in the experiments. We gratefully acknowledge the financial support from a Grant in Aid for Fundamental Scientific Research, Ministry of Education, Culture and Science, Japan.

Nomenclature

C_{Pi} = specific heat of ith layer [J kg^{-1} K^{-1}]
D_i = thermal diffusivity of ith layer [m^2 s^{-1}]
d = characteristic separation distance between anion and cation [m]
d_i = density of ith layer [kg m^{-3}]
e = elementary charge [cgs esu]
$H = R/(d_1C_{P1}l)$ [s^{-1}]
$H' = R'/(d_1C_{P1}l)$ [s^{-1}]
$h = \beta_2 D_2^{1/2}$ [s$^{-1/2}$]
k = Boltzmann constant [J K^{-1}]
L = thickness of the second layer [m]
l = thickness of the first and the third layers [m]
m_i = mass of ith ion [kg]
m^*, m_R, m_S = characteristic mass for a given molten salt [kg]
P_i = momentum of ith ion [kg m s^{-1}]
R = parameter concerning the heat discharge from the metal disk to the atmosphere [J m^{-2} s^{-1} K^{-1}]
R' = parameter concerning the radiation from the first layer to the third layer [J m^{-2} s^{-1} K^{-1}]
r_{ij} = separation distance between ith and jth ions [m, cm]
r_{ix} = x-component of the position vector $\mathbf{r}_i$ [m]
s = argument of Laplace transform [s^{-1}]
T = absolute temperature [K]
T_i = temperature rise in ith layer [K]
T^* = initial temperature rise in the first layer [K]
T^* = reduced form of T
t = time [s]
t^* = reduced form of t
V = volume of the system [m^3]
x = distance measured from the surface of a metal disk [m]
Z_i = valence of ith ion
$\beta_2 = d_2C_{P2}/(d_1C_{P1}l)$ [m^{-1}]
$\Lambda = \psi \exp(-d/\rho)$ [J, erg]
λ_i = thermal conductivity of ith layer [W m^{-1} K^{-1}]
λ = thermal conductivity of molten salt [W m^{-1} K^{-1}]
λ^* = reduced form of λ
λ_0^* = reference term of λ^*
μ, μ_S, μ_R = parameter representing the difference of masses between anion and cation
ξ = parameter concerning the Coulombic potential
$\rho = \rho_{ij}$ for unlike ion pairs [m]
ρ_{ij} = parameter concerning the core repulsive potential between ith and jth ions [m]
ϕ_{ij} = pair potential between ith and jth ions [J, erg]
$\psi = \psi_{ij}$ for unlike ion pairs [J, erg]
ψ_{ij} = parameter concerning the core repulsive potential between ith and jth ions [J, erg]

Literature Cited

Barin, I.; Knacke, O. Tables. In *Thermochemical Properties of Inorganic Substances*; Springer-Verlag: Berlin, Heidelberg, New York, 1973.

Bystrai, G. P.; Desyatnik, V. N.; Zlokazov, V. A. Thermal Conductivity of molten uranium tetrachloride mixed with sodium chloride and potassium chloride. *At. Energ.* **1974**, *36*, 517–518.

Fedorov, V. I.; Machuev, V. I. Thermal Conductivity of Fused Salts. *Teplofiz. Vys. Temp.* **1970**, *8*, 912–914.

Gray, E., Ed. Heat. In *American Institute of Physics Handbook*, 3rd ed.; McGraw-Hill: New York, 1972.

Harada, M.; Tanigaki, M.; Tada, Y. Law of Corresponding States of Uni-univalent Molten Salts. *Ind. Eng. Chem. Fundam.* **1983**, *22*, 116–121.

Harada, M.; Shioi, A.; Uchiyama, Y.; Tada, Y.; Tanigaki, M. "Laser Flash Method for Measuring Thermal Conductivity of Liquids"; Technical Reports of the Institute of Atomic Energy, Kyoto University; No. 202, March 1985.

Janz, G. J. Physical properties. In *Molten Salt Handbook*; Academic Press: New York, 1967; Chapter 1.

Kitade, S.; Kobayashi, Y.; Nagasaka, Y.; Nagashima, A. Measurement of the thermal conductivity of molten KNO_3 and $NaNO_3$ by the transient hot-wire method with ceramic-coated probes. *High Temp.—High Press.* **1989**, *21*, 219–224.

Kubo, R. Statistical-Mechanical Theory of Irreversible Process. I. General Theory and Simple Application to Magnetic and Conduction Problems. *J. Phys. Soc. Jpn.* **1957**, *12*, 570–586.

Lee, H. J.; Taylor, R. E. Determination of Thermophysical Properties of Layered Composites by Flash Method. In *Thermal Conductivity* 14; Plenum Press: New York, 1978; pp 432–434.

Makita, T. Recommended value for thermal conductivity of liquid. In *Busseiteisu*; The Society of Chemical Engineers Japan Ed.; Maruzen: Tokyo, 1964; Vol. 2, Chapter 1 (in Japanese).

McDonald, J.; Davis, H. T. Determination of the Thermal Conductivities of Several Molten Alkali Halides by Means of a Sheathed Hot-Wire Technique. *Phys. Chem. Liq.* **1971**, *2*, 119–134.

Nagasaka, Y.; Nagashima, A. Measurement of the Thermal Diffusivity of Molten KCl up to 1000 °C by the Forced Rayleigh Scattering Method. *Int. J. Thermophys.* **1988**, *9*, 923–931.

Nakazawa, K.; Akahori, M.; Nagasaka, Y.; Nagashima, A. Measurement of Thermal Conductivity of Molten Salts by Means of the Forced Rayleigh Scattering Method—for Alkali Chloride over 1000 °C. *Proc. Natl. Heat Transfer Symp. Jpn.* **1989**, *26th*, 170–172 (in Japanese).

Nakazawa, K.; Nose, M.; Nagasaka, Y.; Nagashima, A. Measurement of Thermal Conductivity of Molten Salts by Means of the Forced Rayleigh Scattering Method—for Alkali Bromide and Alkali Iodide. *Proc. Natl. Heat Transfer Symp. Jpn.* **1990**, *27th*, 400–402 (in Japanese).

Parker, W. J.; Jenkins, R. J.; Butler, C. P.; Abott, G. L. Flash Method of Determining Thermal Diffusivity, Heat Capacity, and Thermal Conductivity. *J. Appl. Phys.* **1961**, *32*, 1679–1684.

Polyakov, P. V.; Gildebrandt, E. M. Investigation of the Thermal Conductivity of Melts of the System KCl-$MgCl_2$. *Teplofiz. Vys. Temp.* **1974**, *12*, 892-893.
Reiss, H.; Mayer, S. W.; Katz, J. L. Law of Corresponding States for Fused Salts. *J. Chem. Phys.* **1961**, *35*, 820-826.
Tada, Y.; Harada, M.; Tanigaki, M.; Eguchi, W. Laser flash method for measuring thermal conductivity of liquids—application to low thermal conductivity liquids. *Rev. Sci. Instrum.* **1978**, *49*, 1305-1314.
Tada, Y.; Harada, M.; Tanigaki, M.; Eguchi, W. Laser Flash Method for Measuring Thermal Conductivity of Liquids. Application to Molten Salts. *Ind. Eng. Chem. Fundam.* **1981**, *20*, 333-336.
Tada, Y.; Hiraoka, S.; Uemura, T.; Harada, M. Corresponding States Correlation of Transport Properties of Uniunivalent Molten Salts. *Ind. Eng. Chem. Res.* **1988**, *27*, 1042-1049.
Tosi, M. P.; Fumi, F. G. Ionic Sizes and Born Repulsive Parameters in the NaCl-Type Alkali Halides—II. *Phys. Chem. Solids* **1964**, *25*, 45-52.
White, L. R.; Davis, H. T. Thermal Conductivity of Molten Alkali Nitrates. *J. Chem. Phys.* **1967**, *47*, 5433-5439.
Young, R. E.; O'Connell, J. P. An Empirical Corresponding States Correlation of Densities and Transport Properties of 1-1 Alkali Metal Molten Salts. *Ind. Eng. Chem. Fundam.* **1971**, *10*, 418-423.

Received for review April 22, 1992
Accepted July 28, 1992

RESEARCH NOTES

Hydrogen-Transferring Liquefaction of Two Different Rank Coals Employing Hydrogenated Anthracene Oil as a Donor Solvent

The liquefaction of two coals, a low-volatile bituminous coal and a lignite, was studied using a hydrogenated anthracene oil as donor solvent. An inert atmosphere was employed to ensure that all the hydrogen incorporated by coal was supplied by hydrogenated compounds from the anthracene oil. Reaction products were separated according to their solubility and the following fractions were obtained: oils, asphaltenes, preasphaltenes, and an unreacted coal organic matter. The amount of hydrogenated compounds in the oil was related to the kinetics of coal solubilization. It compares favorably with the calculated profile of hydroaromatics assuming that only the first hydrogenation derivatives participate in hydrogen donation. An activation energy of about 13 000 K (E/R) was obtained for both coals. For the bituminous coal, 41% of the organic matter was not reactive, whereas for the lignite, the amount of unreactive organic matter was only 26%.

Introduction

At a temperature of above 650 K, coal produces a wide range of pyrolytically generated molecular fragments which, in the absence of a source of hydrogen, undergo reactions leading to a preponderance of gas and char. The stabilization of these coal fragments takes place with hydrogen obtained from three main sources: directly from the gas phase, by chemical rearomatization of hydroaromatic parts of the coal (hydrogen shuttling), or from hydrogenated solvents (hydrogen donation). In this conventional view of a direct liquefaction process, the solvent merely stabilizes the thermally generated radicals without playing any role in promoting bond cleavage. Several researchers have shown that the kinetics of coal conversion is influenced by the amount of hydrogen donor compounds contained in the solvent and have suggested the participation of hydrogenated light molecules in bond scission (Honda and Yamada, 1974; Allen and Gavallas, 1984; McMillen et al., 1987a). A molecular model involving this mechanism has been proposed by McMillen et al. (1987b).

In a donor solvent liquefaction process the concentration of hydrogen donor compounds must be carefully controlled. These molecules must provide enough hydrogen to avoid recondensation of thermally produced radicals and retrogressive reactions leading back to insoluble material. However, an excess has a detrimental effect, increasing gas production and decreasing oil yield. Moreover it has been shown that when hydrogenated substances are in excess, they can react, to give back the aromatic molecule and a naphthenic compound (Mochida and Takeshita, 1980). Both naphthenic and perhydroaromatic compounds exhibit a low donor ability, and therefore, their formation must be avoided.

Extensive work has been performed on coal liquefaction with anthracene oil (Gürüz et al., 1992; Berkowitz et al., 1988; Fabregat et al., 1987) and hydrogenated anthracene oil (Cronauer et al., 1987; Davies et al., 1977; Chiba et al., 1987). The results show that the extraction efficiency of hydrogenated anthracene oil is much greater than that of the fraction prior to treatment for any cut throughout the boiling range. This is clearly due to the presence of a fairly high concentration of polynuclear hydroaromatics. The aim of this work is to determine the effect of the degree of hydrogenation of an anthracene oil on the liquefaction behavior of two different rank coals. The evolution of the solvent composition was related to the kinetics of solubilization. Special attention has been paid to the differences in depletion of hydroaromatic compounds as a function of liquefaction conditions.

Experimental Section

Materials. A light fraction of the anthracene oil was supplied by Industrial Química del Nalón (NalonChem, Spain). The raw material (90% recovered between 215 and 400 °C) was hydrogenated over a sulfided nickel-molybdenum catalyst (BASF, M8-24) to obtain two fractions with a different hydroaromatic compound content. Hydrogenation conditions were temperature 340 °C, hydrogen pressure 100 kg/cm^2, and reaction time 1 h for oil no. 1 and 5 h for oil no. 2. Major components of the hydrogenated solvents are listed in Table I. Details on the analysis are given elsewhere (Rosal et al., 1992). Fraction

0888-5885/92/2631-2407$03.00/0